# Study of the structural and optical properties of InGaAs quantum dots

© A.V. Babichev[1], A.M. Nadtochiy[1,2], S.A. Blokhin[1], V.N. Nevedomsky[1], N.V. Kryzhanovskaya[2], M.A. Bobrov[1], A.P. Vasil'iev[1], N.A. Maleev[1], L.Yu. Karachinsky[3], I.I. Novikov[3], A.Yu. Egorov[3]

[1] Ioffe Institute,
194021 St. Petersburg, Russia
[2] HSE University,
190008 St. Petersburg, Russia
[3] ITMO University,
197101 St. Petersburg, Russia
E-mail: a.babichev@mail.ioffe.ru

*Received April 16, 2024*
*Revised June 17, 2024*
*Accepted August 24, 2024*

The growth parameters of $In_xGa_{1-x}As$ quantum dots grown by molecular-beam epitaxy were tested. It has been shown that a decrease in the indium content in quantum dots structures yields to a decrease in the ground state emission wavelength, with subsequent saturation of the behavior. The use of $In_{0.5}Ga_{0.5}As$ quantum dots makes it possible to realize effective photoluminescence close to 995 nm at 13 K temperature, with emission inhomogeneous broadening of about 57 meV with unimodal size distribution. The high luminescence efficiency for structures with $In_{0.5}Ga_{0.5}As$ quantum dots at 300 K temperature has been demonstrated, which makes it possible to use this type of active regions for the fabrication of vertical microcavities to further realize reservoir computing.

**Keywords:** molecular-beam epitaxy, gallium arsenide, InGaAs, Stranski-Krastanov mode.

DOI: 10.61011/SC.2024.06.59453.6287

## 1. Introduction

Active regions based on quantum dots (QDs) are used to form various types of laser structures, including optically pumped structures with vertical microcavities [1–7]. These structures are formed by positioning a light-emitting active region between two distributed Bragg reflectors (DBRs). Low-temperature lasing has already been demonstrated at 77 K under optical pumping in micropillar lasers with a vertical microcavity and extremely low (several tens of $\mu$W) threshold pump powers [8]. This was achieved through the use of $Al_{0.2}Ga_{0.8}As/Al_{0.9}Ga_{0.1}As$ DBRs, which are non-absorbing at the optical pumping wavelength (700−820 nm), and active regions with a single QD layer. A further increase in the operating temperature of these microlasers necessitates an increase in the optical gain of active regions and, consequently, a transition to the designs with three QD layers [9–11]. This approach allowed the experimenters to achieve lasing in microlasers with a vertical microcavity and three QD layers at a temperature of 130 K [9].

A high spectral uniformity of microlasers in an array ($\sim 200\,\mu$eV in an array of $8 \times 8$ elements [10]) is needed to implement reservoir computing based on arrays of optically pumped microlasers. The use of quantum wells (QWs) as the active region of optically pumped microlasers is limited by the significant contribution of nonradiative recombination on the side surface of a microlaser [10,12]). QDs allow one to suppress markedly the effect of nonradiative recombination and to implement a sufficiently wide gain spectrum for efficient tuning of the lasing wavelength in an array of microlasers [10,13–16]. At the same time, if the QD deposition conditions are not optimized, a parasitic bimodality effect (i.e., the formation of two types of QDs), which has a negative influence on the PL intensity and broadens the emission spectrum significantly [17,18], may be observed in an array.

The metal-organic chemical vapor deposition (MOCVD) technique helps avoid the emergence of bimodality in an InGaAs QD array [8–10]. Photoluminescence (PL) with a full width at half-maximum ($FWHM$) of its spectrum of $\sim 50$ meV has already been demonstrated at an ultra-low optical pumping density ($\sim 1.7$ mW/cm$^2$) and a temperature of 13 K [16]. In addition, the micro-PL spectra measured at medium optical pumping densities ($\sim 350$ W/cm$^2$) are characterized by FWHM values of 20−25 meV at a temperature of 10 K [19]) and $\sim 60-80$ meV at 290 K [10,19,20].

The main disadvantage of MOCVD is the significant variation of thickness of layers of the microcavity structure over the wafer area ($\sim 2\%$ [21]), which translates into a wavelength spread for the vertical microcavity ($\sim 29$ meV) over the area of a two-inch wafer [10]. A high spectral non-uniformity of the microcavity wavelength is thus observed in an array of microlasers ($\sim 260\,\mu$eV for an array of $30 \times 30$ microlasers with a diameter of $4\,\mu$m and a pitch of $8\,\mu$m). Therefore, when the MOCVD growth method is used, additional precision compensation of the microlaser diameter in an array via electron-beam lithography is needed [10] to adjust the lasing wavelength and implement diffraction coupling of microlasers in the array.

Molecular-beam epitaxy (MBE) provides a lower non-uniformity of layer thicknesses over the wafer area ($< 1\%$). To achieve lasing with a vertical microcavity, one needs to increase the gain of an active region based on QDs formed by MBE. Thus, it is necessary to maintain efficient QD PL at a wavelength of 1100 nm at a temperature of 300 K.

The growth of InAs and InGaAs QDs of this spectral range has been reported in literature. When an InAs layer is deposited, 2D−3D transformation is typically observed (depending on the growth temperature and the flux of group III elements) at a critical thickness of $\sim 1.4-1.7$ monolayers (MLs). Specifically, it was demonstrated in [22] that the initial InAs QDs formed from a bulk InAs layer with a thickness of 1.67 ML exhibit low-temperature PL near 986 nm (at a temperature of 77 K) with a significant inhomogeneous broadening ($FWHM \sim 75$ meV). Since PL with a maximum around 1114 nm at 77 K ($FWHM \sim 50$ meV [22]) is observed when the InAs thickness increases to 2.33 ML, the calculated InAs thickness needed to implement PL in the required spectral range (1000 nm at 77 K and 1100 nm at 300 K) is $\sim 1.73$ ML. A QD array was found to be highly sensitive to the substrate temperature and the amount of InAs deposited during growth in preliminary experiments. Thus, the use of initial InAs QDs of this spectral range leads to a lower (compared to InGaAs QDs [23]) peak PL intensity and a greater non-uniformity of parameters over the wafer.

Studies into the formation of QDs with the use of the method of partial capping and high-temperature annealing [15], which was proven to be efficient [24,25], were performed with the aim of reducing the magnitude of inhomogeneous broadening in an InGaAs QD array. Intense PL at a wavelength of 1100 nm was demonstrated at 300 K with a small spread of the microcavity wavelength over the wafer area ($\sim 14$ meV, while MOCVD provided $\sim 29$ meV [10]). However, the Stranski–Krastanov growth of QDs from a bulk $In_{0.63}Ga_{0.37}As$ layer with partial capping and high-temperature annealing led to bimodality in the InGaAs QD array with a characteristic FWHM value of $\sim 73$ meV [16] measured at an optical pumping density of 1.7 mW/cm$^2$ and a temperature of 13 K.

In the present study, we report on the specifics of formation and the parameters of inhomogeneous broadening in an array of InGaAs QDs grown by MBE in the Stranski–Krastanov mode. A vertical microcavity with an active region of this type was formed, and its structural quality was investigated.

## 2. Experimental samples

Heterostructures with InGaAs QDs were grown using the MBE method in the Stranski–Krastanov mode by depositing an InGaAs layer of a certain effective thickness at an arsenic ($As_4$) pressure of $2 \cdot 10^{-7}$ Torr. The GaAs substrate temperature in the process of QD deposition was 485°C, while the remaining epitaxial layers were grown at a temperature of 600°C. The thickness of the GaAs capping layer was increased from 5 nm [15] to 10 nm. The QD layers were positioned in the middle of a 300-nm-thick GaAs matrix layer, which was located between two $Al_{0.23}Ga_{0.77}As$ barriers with a thickness of 35 nm.

The critical InGaAs layer thickness corresponding to the transition from layer-by-layer growth to three-dimensional growth (2D−3D transformation) was identified by monitoring the time of transformation of the reflection high-energy electron diffraction (RHEED) pattern. As was demonstrated in [26], the critical InGaAs layer thickness increases as the amount of indium in InGaAs QDs decreases. The $In_{0.5}Ga_{0.5}As$ composition was chosen for QD deposition in the first test heterostructure. The deposited $In_{0.5}Ga_{0.5}As$ layer thickness was set by adjusting the experimental time interval to a certain value exceeding the 2D−3D transformation time. With the 2D−3D transformation time exceeded by 20%, the ground-state peak in the PL spectrum measured at room temperature was positioned at $\sim 1120$ nm; when the 2D−3D transformation time was exceeded by 10%, the PL peak shifted toward shorter wavelengths (to $\sim 1074$ nm). Since further shortening of the time interval is associated with a high non-uniformity of the QD array over the wafer area, a 10% excess over the 2D−3D transformation time was chosen for experiments. A series of experimental samples with $In_xGa_{1-x}As$ QD layers with the indium content (fraction $x$) varying within the range of 45−60% (in 5% increments) were grown to obtain a ground-state PL line near 1000 nm at a temperature of 13 K. The InGaAs layer deposition rate was (0.85−1.13) ML/s for samples with $In_xGa_{1-x}As$ QD layers with the indium content varying within the range of 45−60%. The resulting estimated InGaAs layer thickness was 6.6, 5.5, 4.7, and 4 ML for structures with $In_xGa_{1-x}As$ QDs with an indium content of 45, 50, 55, and 60%.

With the epitaxy of heterostructures of active regions with $In_xGa_{1-x}As$ QDs optimized, epitaxial growth of a heterostructure with a vertical microcavity was performed. The bottom DBR included 35 pairs of alternating quarter-wave ($\lambda/4n$) $Al_{0.2}Ga_{0.8}As/Al_{0.9}Ga_{0.1}As$ layers. A vertical microcavity with a thickness of $\lambda/n \sim 300$ nm was formed based on GaAs with three layers of $In_{0.5}Ga_{0.5}As$ QDs, which are needed to increase the optical gain of the active region, positioned at its center. The QD layers were separated by 20-nm-thick GaAs layers. The top DBR was formed from 27 pairs of alternating $Al_{0.2}Ga_{0.8}As/Al_{0.9}Ga_{0.1}As$ layers. The calculated position of the resonant wavelength of the microcavity (dip in the reflection spectrum) was 978 nm at a temperature of 13 K.

Transmission electron microscopy (TEM) studies of the vertical microcavity heterostructure were performed using a JEM2100F (Jeol) electron microscope under an accelerating voltage of 200 kV. Cross-section samples were prepared in accordance with the conventional procedure that includes thinning by precision grinding and sputtering with argon ions to perforation at the final stage.

The maps of surface defects of the vertical microcavity heterostructure were examined using a Surfscan KLA Tencor automated system for surface condition monitoring and determining the density of defects.

PL spectra of heterostructures with InGaAs QDs were measured under continuous optical pumping by a YAG:Nd laser with a lasing wavelength of 532 nm and an output radiation power of 150 mW (the excitation power density was $\sim 5\,\mathrm{kW/cm^2}$). PL was recorded in the standard lock-in detection mode with the use of a cooled germanium diode and an MDR-23 monochromator. The measurement of PL spectra at 13 K was performed using a Janis closed-cycle helium cryostat within a wide range of optical pumping. Low-temperature studies of PL spectra allow one to suppress the processes of thermal ejection and recapture of carriers (i. e., suppress carrier transport). The contribution of excited states may be minimized by reducing the pump level. The optical pumping density was adjusted using a set of neutral optical filters; the variation range was $(1-3\cdot 10^{-6})$. The minimum excitation power density was $\sim 1.7\,\mathrm{mW/cm^2}$. The measurements of PL spectra at a temperature of 300 K were carried out at an excitation power of 0.45 mW, which corresponded to an excitation power density of $\sim 15\,\mathrm{W/cm^2}$.

Reflectance spectra maps for the vertical microcavity heterostructure were recorded at a temperature of 297 K using a VerteX PM2000 setup (Nanometrics Inc.).

## 3. Results and discussion

The results of PL spectra measurements performed within a wide spectral range at a minimum optical pumping density are presented in Figure 1. It is evident that with a high indium content ($\geq 55\%$) of QDs and a decreasing pumping density, the PL spectrum ceases to change in shape at a certain density level and preserves its form of a superposition of several peaks even at the weakest pumping, which is indicative of bimodality of this InGaAs QD array. The absolute FWHM values of the PL spectra corresponding to an ultra-low optical pumping density ($\sim 1.7\,\mathrm{mW/cm^2}$) were 81 and 68 meV for the structures with $In_xGa_{1-x}As$ QDs containing 60 and 55% of indium.

It was demonstrated in [16] that the deposition of QDs from a bulk $In_{0.63}Ga_{0.37}As$ layer with partial capping and high-temperature annealing led to bimodality in the InGaAs QD array grown by MBE. The FWHM value corresponding to the low-temperature PL spectrum was 73 meV at an optical pumping density of $1.7\,\mathrm{mW/cm^2}$ [16].

With the indium content reduced to 45–50%, the FWHM value of PL spectra of the examined structures with $In_xGa_{1-x}As$ QDs decreased, and the PL spectra themselves became more symmetrical (Figure 1), indicating that PL through the ground state was predominant. The FWHM values of the PL spectra corresponding to an ultra-low optical pumping density ($\sim 1.7\,\mathrm{mW/cm^2}$) were $\sim 57$ meV for both heterostructures with $In_xGa_{1-x}As$ QDs containing 50 and 45% of indium.

PL spectra were measured at a temperature of 300 K and an excitation power of $\sim 0.45$ mW, which corresponded to an excitation power density of $\sim 15\,\mathrm{W/cm^2}$, in order to evaluate the PL efficiency that characterizes the optical gain of the active region. The results are presented in Figure 2. A peak corresponding to PL of InGaAs QDs and a PL peak of the wetting layer (close to 920 nm) are seen in the spectra. The $FWHM$ of PL spectra of all the examined structures falls within the range of 64–74 meV, which is attributable to the contribution of excited states and agrees with the values reported earlier [19].

The results obtained at 13 (Figure 1) and 300 K (Figure 2) under similar pump densities ($15\,\mathrm{W/cm^2}$) were compared. It turned out that the $FWHM$ of the PL line for the structure with $In_xGa_{1-x}As$ QDs with an indium content of 60% decreases from 80 to 70 meV with increasing temperature. The structure with $In_xGa_{1-x}As$ QDs with an indium content of 55% behaved in a similar way when the temperature increased: the FWHM of the PL line decreased from 72 to 64 meV. In contrast, the $FWHM$ of the PL line for the structures with $In_xGa_{1-x}As$ QDs with an indium content of 50 and 45% increased from 64 to 71 meV and from 61 to 64 meV, respectively, with increasing temperature.

In general, carriers are distributed randomly over the QD array states at low temperatures. When the temperature increases, the ejection of carriers from smaller QDs (with weak carrier localization) with subsequent capture through the wetting layer into larger QDs becomes possible. This process manifests itself in a reduction of the $FWHM$ value of the PL spectrum within the temperature range of 140–150 K. A subsequent temperature growth leads to an equilibrium distribution of carriers over the QD array states and an increase in $FWHM$ of the PL spectrum. Thus, the ratio of small and large QDs governs the temperature behavior of $FWHM$ of the PL spectrum. In QDs with bimodality (two ensembles of QDs differing in size), the $FWHM$ value decreases significantly with increasing temperature [27]. In contrast, QDs with weak inhomogeneous broadening exhibit a slight increase in $FWHM$ of the PL peak when the temperature rises.

Thus, the last two structures have the temperature behavior of $FWHM$ characteristic of structures without the effect of QD bimodality ($FWHM$ remains constant or increases slightly with temperature). This provides an additional confirmation of the conclusion regarding the presence of bimodality in InGaAs QDs containing $\geq 55\%$ of indium, which was formulated based on the results of analysis of Figure 1 (see above).

The PL data obtained for the reference structure with QDs deposited by MBE from a bulk $In_{0.63}Ga_{0.37}As$ layer with partial capping and high-temperature annealing [15] are also presented in Figure 2. It follows from the figure that, compared to the reference structure with QDs containing 63% of indium, the maximum of the PL spectrum for

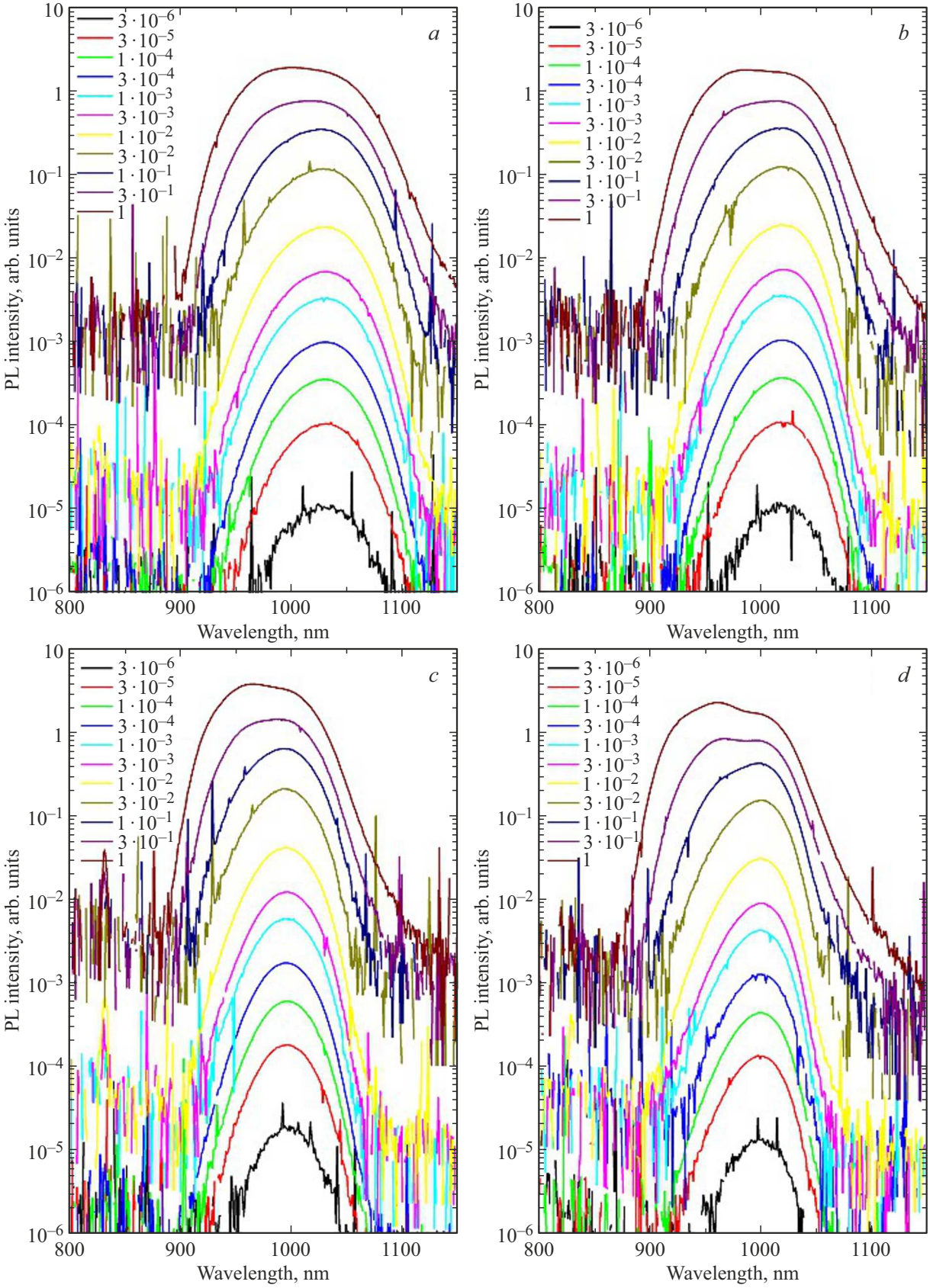


**Figure 1.** PL spectra (semi-logarithmic scale) of structures with $In_xGa_{1-x}As$ QDs with a varying indium content (fraction $x$) measured at a temperature of 13 K. The coefficients of pump laser power attenuation were as follows: $3 \cdot 10^{-6}$, $3 \cdot 10^{-5}$, $1 \cdot 10^{-4}$, $3 \cdot 10^{-4}$, 0.001, 0.003, 0.01, 0.03, 0.1, 0.3, and 1.0. The plots in panels *a, b, c*, and *d* correspond to the structures containing 60, 55, 50, and 45% of indium, respectively. (A color version of the figure is provided in the online version of the paper).

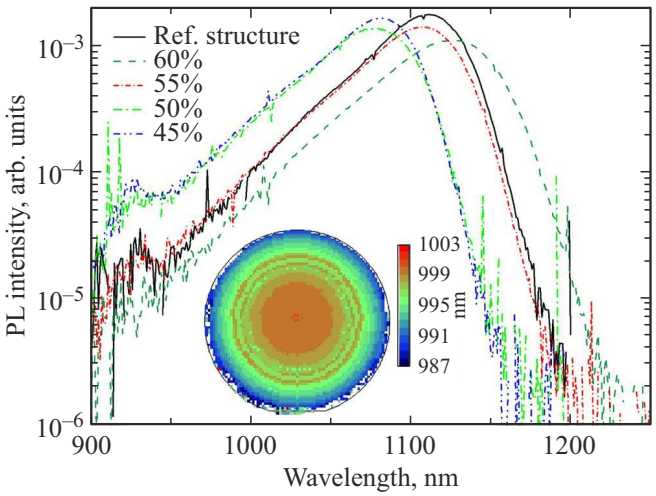


**Figure 2.** PL spectra (semi-logarithmic scale) of heterostructures with $In_xGa_{1-x}As$ QDs with a varying (60, 55, 50, 45%) indium content (fraction $x$) measured at a temperature of 300 K. The PL spectrum of the reference structure with QDs containing 63% of indium is also shown. The inset shows reflectance spectra mapped over the area of a three-inch wafer of the vertical microcavity heterostructure. (A color version of the figure is provided in the online version of the paper).

the heterostructure with 60% of indium in QDs is shifted toward longer wavelengths, which is attributable to the difference in thickness of the capping layer; notably, the absolute maximum PL intensity is somewhat lower. It should also be noted that the PL maximum shifts toward shorter wavelengths as the indium content in InGaAs QD layers decreases gradually from 60 to 45%. The ground-state PL line for the heterostructure with InGaAs QDs with 50% of indium corresponds to a wavelength of 1077 nm. The PL intensity may be increased through the use of a capping layer (e.g., $In_{0.48}Ga_{0.52}P$) with a bandgap wider (1.92 eV) than the one of GaAs [20] and by increasing the QD density due to the formation of an additional $In_yGa_{1-y}As$ layer prior to the deposition of the $In_xGa_{1-x}As$ layer for QD fabrication.

The study of reflectance spectra mapped over the area of a three-inch wafer (see the inset in Figure 2) revealed that the position of the resonant wavelength of the microcavity varies only slightly along the trajectory from the edge to the center of the three-inch wafer (within $\sim 12$ meV). According to the results of numerical modeling, this corresponds to a $\sim 1\%$ thickness deviation. The resonant wavelength of the microcavity was shifted by 3.8 meV at a distance of 25 mm from the center. In earlier studies of a MOCVD vertical microcavity structure with 27 and 23 $Al_{0.9}Ga_{0.1}As$/GaAs pairs forming a DBR, the position of the resonant wavelength of the microcavity varied along the trajectory from the edge to the center of a two-inch wafer within $\sim 29$ meV [10], which corresponds to a 2.6% layer thickness deviation.

It was demonstrated in [10] that only 20 of the 64 micropillar structures ($\sim 31\%$) in an array after etching fit within a $\pm 100\,\mu$eV spectral range of positions of the resonant wavelength of the microcavity. Thus, the reduction of spectral spread in the MBE-grown structure examined in the present study should translate into a greater fraction (91%) of micropillars in the array that fit within the spectral range of $\pm 100\,\mu$eV. Therefore, it should be possible to implement diffraction coupling in an array of $8 \times 8$ elements with only six microlasers requiring precision diameter compensation.

The results of examination of the structural quality of the obtained vertical microcavity heterostructure with an active region based on three layers of $In_{0.5}Ga_{0.5}As$ QDs with a transmission electron microscope are presented in Figure 3. It is evident that the active region is defect-free and the layers are planar. Just as in the earlier study of QDs deposited from a bulk $In_{0.63}Ga_{0.37}As$ layer with partial capping and high-temperature annealing [15], the effect of stacking (vertical alignment) of QDs located in different layers is observed in the heterostructure. The scanning transmission electron microscopy (STEM) image was obtained at minimum magnification to provide an overall

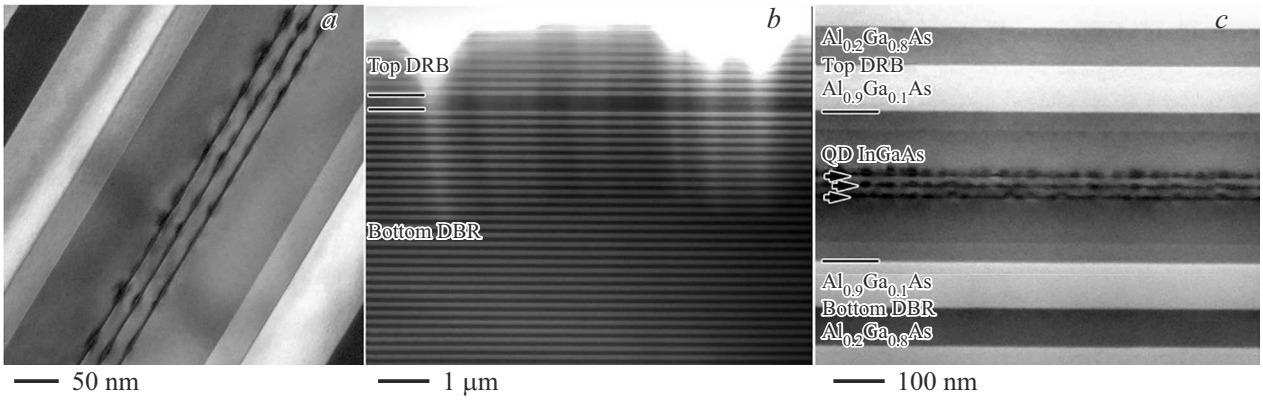


**Figure 3.** *a* — active region of the heterostructure imaged by transmission electron microscopy; *b* and *c* — QDs in the vertical microcavity heterostructure imaged by scanning transmission electron microscopy.

view of the structure. The DBR layers are characterized by fine planarity and a constant period, and no defects were detected at the DBR/active region interfaces.

As was demonstrated earlier, the use of MBE in the process of overgrowth does not lead to planarization of an uneven surface (buried tunnel junction) [28,29]. A similar effect may be observed when a QD array is buried in the vertical microcavity heterostructure. Moreover, the surface roughness may increase (in comparison with mirrors based on $GaAs/Al_{0.9}Ga_{0.1}As$) as a result of epitaxial growth of DBR layers with an elevated aluminum content ($Al_{0.2}Ga_{0.8}As/Al_{0.9}Ga_{0.1}As$) due to gallium segregation on the surface [30]. Surface defect maps were plotted in order to study the surface quality of the vertical microcavity heterostructure. The measured densities of normal defects ($0.6-10\,\mu m^2$ in size) and oval defects ($10-250\,\mu m^2$ in size) were 461 and 222 units/cm$^2$, respectively, which is consistent with the results presented earlier [31]. The haze value, which characterizes surface roughness, was 22 and 3 units/million for normal and oval defects. One may estimate root-mean-square (rms) surface roughness $\delta$ based on these data with the use of the following expression [32]: $\delta = (\lambda/4 \cdot \pi)(H/R_0)^{0.5}$, where $R_0$ is the reflectance of the material, $H$ is the haze value, and $\lambda$ is the pumping wavelength. The estimated root-mean-square surface roughness of the fabricated heterostructures did not exceed 0.3 nm for normal defects. In addition, $\delta$ is near-zero for oval defects. Thus, an atomically smooth surface of the top DBR based on the $Al_{0.2}Ga_{0.8}As/Al_{0.9}Ga_{0.1}As$ heteropair was obtained in experiments.

## 4. Conclusion

The modes of formation of $In_xGa_{1-x}As$ quantum dots by molecular-beam epitaxy were optimized. It was demonstrated that the ground-state luminescence wavelength gets shorter as the indium content in structures with $In_xGa_{1-x}As$ QDs decreases (with eventual saturation of this dependence). The use of QDs formed from an $In_{0.5}Ga_{0.5}As$ layer allowed for intense low-temperature photoluminescence with a maximum around 995 nm and a characteristic $FWHM$ of the PL peak of $\sim 57$ meV; notably, the bimodality effect in the QD array was not detected. Epitaxial growth of a vertical microcavity heterostructure with an active region based on three layers of $In_{0.5}Ga_{0.5}As$ QDs was performed. The high structural perfection of the vertical microcavity heterostructure and the lack of influence of DBR layers with an increased aluminum content ($Al_{0.2}Ga_{0.8}As/Al_{0.9}Ga_{0.1}As$) on the surface roughness of the heterostructure were verified via transmission electron microscopy and analysis of surface defect distribution maps. The discussed vertical microcavity design is the first to achieve low-threshold surface whispering-gallery mode lasing [33] and vertical mode lasing at elevated temperatures [34].

### Funding

The work on structure design, epitaxy of heterostructures, TEM imaging, and photoluminescence spectra measurement performed by researchers from the Ioffe Institute of the Russian Academy of Sciences was supported by grant No. 22-19-00221 from the Russian Science Foundation, https://rscf.ru/project/22-19-00221/. N.V. Kryzhanovskaya and A.M. Nadtochii wish to thank the HSE Fundamental Research Program for supporting their work on analysis of photoluminescence spectra. The authors from ITMO University express their gratitude to the Ministry of Science and Higher Education of the Russian Federation, research project No. 2019-1442 (research topic code FSER-2020-0013), for support of the analysis of surface defect maps and reflectance spectra of the vertical microcavity heterostructure.

### Conflict of interest

The authors declare that they have no conflict of interest.

## References

[1] P. Senellart, G. Solomon, A. White. Nature Nanotechnol., **12** (11), 1026–1039 (2017).
[2] S. Kreinberg, T. Grbešić, M. Strauß, A. Carmele, M. Emmerling, C. Schneider, S. Höfling, X. Porte, S. Reitzenstein. Light: Sci. Appl., **7** (1), Art.# 41 (2018).
[3] H. Deng, G.L. Lippi, J. Mørk, J. Wiersig, S. Reitzenstein. Adv. Opt. Mater., **9** (19), Art.# 2100415 (2021).
[4] M. Lermer, N. Gregersen, M. Lorke, E. Schild, P. Gold, J. Mørk, C. Schneider, A. Forchel, S. Reitzenstein, S. Høfling, M. Kamp. Appl. Phys. Lett., **102** (5), Art.# 052114 (2013).
[5] S. Kreinberg, W.W. Chow, J. Wolters, C. Schneider, C. Gies, F. Jahnke, S. Höfling, M. Kamp, S. Reitzenstein. Light: Sci. Appl., **6** (8), Art.# e17030 (2017).
[6] B. Bahari, A. Ndao, F. Vallini, A. El Amili, Y. Fainman, B. Kanté. Science, **358** (6363), 636 (2017).
[7] N. Heermeier, T. Heuser, J. Große, N. Jung, A. Kaganskiy, M. Lindemann, N.C. Gerhardt, M.R. Hofmann, S. Reitzenstein. Laser Photon. Rev., **16** (4), Art.# 2100585 (2022).
[8] C.-W. Shih, I. Limame, S. Krüger, C.C. Palekar, A. Koulas-Simos, D. Brunner, S. Reitzenstein. Appl. Phys. Lett., **122** (15), Art.# 151111 (2023).
[9] L. Andreoli, X. Porte, T. Heuser, J. Große, B. Moeglen-Paget, L. Furfaro, S. Reitzenstein, D. Brunner. Opt. Express, **9** (6), 9084 (2021).
[10] T. Heuser, J. Grose, S. Holzinger, M.M. Sommer, S. Reitzenstein. IEEE J. Select. Top. Quant. Electron., **26** (1), 1 (2020).
[11] K. Gaur, C.-W. Shih, I. Limame, A. Koulas-Simos, N. Heermeier, C.C. Palekar, S. Tripathi, S. Rodt, S. Reitzenstein. Appl. Phys. Lett., **124** (4), Art.# 041104 (2024).
[12] D. Ouyang, N.N. Ledentsov, D. Bimberg, A.R. Kovsh, A.E. Zhukov, S.S. Mikhrin, V.M. Ustinov. Semicond. Sci. Technol., **18** (12), L53 (2003).
[13] H.L. Wang, D. Ning, S.L. Feng. J. Cryst. Growth, **209** (4), 630 (2000).

[14] S. Liang, H.L. Zhu, W. Wang. J. Appl. Phys., **100** (10), Art.# 103503 (2006).
[15] A.V. Babichev, S.D. Komarov, Yu.S. Tkach, V.N. Nevedomskiy, S.A. Blokhin, N.V. Kryzhanovskaya, A.G. Gladyshev, L.Ya. Karachinsky, I.I. Novikov. Semiconductors, **57** (1), 58 (2023).
[16] A.V. Babichev, S.D. Komarov, J.S. Tkach, N.V. Kryzhanovskaya, A.M. Nadtochiy, A.A. Blokhin, S.A. Blokhin, V.N. Nevedomskiy, N.A. Maleev, A.G. Gladyshev, L.Ya. Karachinsky, I.I. Novikov. *Proc. of 2022 Intern. Conf. on Electrical Engineering and Photonics* (*EExPolytech*) (St. Petersburg, Russia, 2022).
[17] G. Saint-Girons, G. Patriarche, L. Largeau, J. Coelho, A. Mereuta, J.M. Moison, J.M. Gérard, I. Sagnes. Appl. Phys. Lett., **79** (14), 2157 (2001).
[18] H. Kissel, U. Müller, C. Walther, W.T. Masselink, Yu.I. Mazur, G.G. Tarasov, M.P. Lisitsa. Phys. Rev. B, **62** (11), 7213 (2000).
[19] B. Kamiński, A. Zielińska, A. Musiał, C.W. Shih, I. Limame, S. Rodt, S. Reitzenstein, G. Sęk. arXiv preprint arXiv:2305.04938
[20] I. Kaiander. PhD. Thesis. *MOCVD growth of InGaAs/GaAs QDs for long wavelength lasers and VCSELs* (Berlin, Technischen Universität Berlin, 2005). Accessed online: https://api-depositonce.tu-berlin.de/server/api/core/bitstreams/2e5ff7d1-9b4f-47d0-8aff-1133b0b8dad1/content (due to 16.04.2024).
[21] 10.1063/1.5050669 T. Heuser, J. Große, A. Kaganskiy, D. Brunner, S. Reitzenstein. APL Photonics, **3** (11), Art. #116103 (2018).
[22] A.Yu. Egorov. Candidate's Dissertation in Mathematics and Physics *Pryamoe poluchenie poluprovodnikovykh kvantovykh provolok i tochek metodom molekulyarno-puchkovoi epitaksii* (SPb., Fiz.-Tekh. Inst., 1996) (in Russian).
[23] K. Watanabe, T. Akiyama, Y. Yokoyama, K. Takemasa, K. Nishi, Y. Tanaka, M. Sugawara, Y. Arakawa. J. Cryst. Growth, **378**, 627 (2013).
[24] H. Sasakura, S. Kayamori, S. Adachi, S. Muto. J. Appl. Phys., **102** (1), Art.# 013515 (2007).
[25] J.M. García, T. Mankad, P.O. Holtz, P.J. Wellman, P.M. Petroff. Appl. Phys. Lett., **72** (24), 3172 (1998).
[26] V.M. Ustinov, A.E. Zhukov, A.Y. Egorov, N.A. Maleev. *Quantum Dot Lasers* (Oxford, Oxford University Press, 2003).
[27] A.V. Babichev, A.M. Nadtochiy, Y.S. Tkach, N.V. Kryzhanovskaya, S.A. Blokhin, V.N. Nevedomskiy, A.G. Gladyshev, N.A. Maleev, L.Ya. Karachinsky, I.I. Novikov. J. Phys. Math., **69** (3.2), 50 (2023).
[28] S.A. Blokhin, A.V. Babichev, A.G. Gladyshev, L.Ya. Karachinsky, I.I. Novikov, A.A. Blokhin, M.A. Bobrov, N.A. Maleev, V.V. Andryushkin, D.V. Denisov, K.O. Voropaev, I.O. Zhumaeva, V.M. Ustinov, A.Yu. Egorov, N.N. Ledentsov. IEEE J. Quant. Electron., **58** (2), 1 (2022).
[29] M. Muller, P. Debernardi, C. Grasse, T. Grundl, M.-C. Amann. IEEE Phot. Techn. Lett., **25** (2), 140 (2013).
[30] W. Braun, K.H. Ploog. J. Appl. Phys., **75** (4), 1993 (1994).
[31] A.V. Babichev, A.G. Gladyshev, D.V. Denisov, V.V. Dyudelev, D.A. Mikhailov, S.O. Slipchenko, A.V. Lyutetskii, L.Ya. Karachinsky, I.I. Novikov, A.Yu. Andreev, I.V. Yarotskaya, K.A. Podgaetskii, A.A. Marmalyuk, A.A. Padalitsa, M.A. Ladugin, N.A. Pikhtin, G.S. Sokolovskii, A.Yu. Egorov. Tech. Phys. Lett., **48** (15), 83 (2022).
[32] A. Steinbach, A. Belyaev, B. Pinto, D. Chen, S. Radovanovic, G. Neskovic, H. Yeh, A. Wang, J. Cao, J. Reich, D. Kavaldjiev, P. Dighe, R. Bammi, L. Vintro, D. Bloom. *Be market ready*, ed. by U. Subramaniam. Yield management solutions (KLA-Tencor Corporation, San Jose, California, 2006) p. 64. Available online: https://issuu.com/kla-tencor/docs/summer06 (due to 16.04.2024)
[33] A. Babichev, I. Makhov, N. Kryzhanovskaya, S. Troshkov, Y. Zadiranov, Y. Salii, M. Kulagina, M. Bobrov, A. Vasilev, S. Blokhin, N. Maleev, L. Karachinsky, I. Novikov, A. Egorov. arXiv preprint arXiv:2407.02196. (2024). https://doi.org/10.48550/arXiv.2407.02196
[34] A. Babichev, I. Makhov, N. Kryzhanovskaya, A. Blokhin, Y. Zadiranov, Y. Salii, M. Kulagina, M. Bobrov, A. Vasiliev, S. Blokhin, N. Maleev, M. Tchernycheva, L. Karachinsky, I. Novikov, A. Egorov. arXiv preprint arXiv:2407.16271. (2024). https://doi.org/10.48550/arXiv.2407.16271

*Translated by D.Safin*